Geophysical Research Letters

RESEARCH LETTER
10.1029/2024GL110228

Solar Energetic Electron Access to the Moon Within the Terrestrial Magnetotail and Shadowing by the Lunar Surface

Lucas Liuzzo[1], Andrew R. Poppe[1], Christina O. Lee[1], and Vassilis Angelopoulos[2]

[1]Space Sciences Laboratory, University of California, Berkeley, CA, USA, [2]Department of Earth, Planetary, and Space Sciences, University of California, Los Angeles, CA, USA

Key Points:

- High-energy solar energetic electrons (SEEs) have direct access to the lunar environment when in the terrestrial magnetotail
- Precipitation onto the lunar nightside carves-out electrons from the ambient distribution, generating extended shadows far from the Moon
- When in the tail, the lunar surface is non-uniformly bombarded by Earthward-traveling SEEs, with reduced access to the dayside hemisphere

Supporting Information:

Supporting Information may be found in the online version of this article.

Correspondence to:

L. Liuzzo,
liuzzo@berkeley.edu

Citation:

Liuzzo, L., Poppe, A. R., Lee, C. O., & Angelopoulos, V. (2024). Solar energetic electron access to the Moon within the terrestrial magnetotail and shadowing by the lunar surface. *Geophysical Research Letters*, *51*, e2024GL110228. https://doi.org/10.1029/2024GL110228

Received 9 MAY 2024
Accepted 20 JUL 2024

Abstract We present measurements of 30–700 keV Solar Energetic Electrons (SEEs) near the Moon when within the terrestrial magnetotail by the *Acceleration, Reconnection, Turbulence, and Electrodynamics of the Moon's Interaction with the Sun* spacecraft. Despite their detection deep within the tail, the incident flux and spectral shape of these electrons are nearly identical to measurements taken upstream of Earth in the solar wind by the Wind spacecraft; however, their pitch angle distribution is isotropized compared to the more field-aligned distribution upstream. We illustrate that SEEs initially traveling Earthward precipitate onto the lunar far-side, generating extended shadows in the cis-lunar electron distribution. By modeling the dynamics of these electrons, we show that their precipitation patterns on the lunar near-side are comparatively reduced. The non-uniform precipitation and accessibility of potentially hazardous electrons to the Moon's surface are highly relevant in the context of astronaut safety during the planned exploration of the lunar environment.

Plain Language Summary The Moon is located within the tail of Earth's magnetosphere during one-third of its orbit. Although the strong terrestrial magnetic field prevents high-energy particles from reaching Earth's surface, the Moon does not receive the same protection when it is within the terrestrial magnetotail. Instead, we show that the high-energy electron flux near the Moon is unchanged during intense solar energetic electron events compared to measurements taken far upstream of Earth. However, the precipitation of these particles onto the lunar surface is non-uniform. Since these electrons gain access to the magnetosphere from down-tail of the Moon, they preferentially bombard the lunar far-side surface. This creates a shadow in the electrons on the nearside that extends far beyond the Moon toward Earth. Hence, despite the high flux of these particles that are potentially hazardous to future activities on the lunar surface, there exist regions across the lunar near-side where the relative flux of these electrons is reduced relative to the upstream value when the Moon is within the magnetotail. These findings provide context for the fundamental scientific understanding of high-energy solar electrons and their access to the lunar surface.

1. Introduction

During the Moon's (radius R_L = 1,737.4 km) 29.5-day synodic period as it orbits Earth, it passes through the terrestrial magnetotail for ∼1 week. Here, the lunar environment is ostensibly shielded from the low-energy solar wind plasma and is instead exposed to the tenuous plasma comprising the tail (e.g., Liuzzo, Poppe, & Halekas, 2022; Terada et al., 2017) nearly ∼60R_E from Earth (radius R_E = 6,378 km). However, besides the solar wind, the Sun is also a source of high-energy ions and electrons that are associated with flares and coronal mass ejections (CMEs). Recently, Liuzzo et al. (2023) found that solar energetic protons have nearly unrestricted access to the Moon while embedded within the terrestrial magnetotail. However, there are few studies investigating solar energetic electron (SEE) access to the lunar environment within the tail. Recently, Jordan et al. (2023) estimated that incident electrons at energies below 100s of MeV would be deflected by the tail since their gyroradii are small on the scales of the magnetotail. Hence, they suggest that the Moon may not be exposed to any SEEs during each magnetotail transit. This contradicts observations from Explorer 35 spacecraft which detected SEEs within the magnetotail at energies as low as ∼50 keV (e.g., Lin, 1968; Van Allen & Ness, 1969).

Therefore, understanding and quantifying the accessibility of high-energy electrons to the Moon's surface within the magnetotail is imperative for characterizing the lunar environment. In addition, constraining the resulting surface fluxes is critical when investigating potential hazards to astronauts during future missions to the Moon. We present a case study of two SEE events where the Moon was bombarded by a population of high-energy

electrons when located within the tail. By comparing observations within the tail to concurrent measurements taken upstream of Earth, we find that the tail is a poor shield to the incident electrons, resulting in little-to-no change to the local fluxes. However, their pitch angle distributions (PADs) are altered from highly field-aligned upstream of Earth to isotropic at most locations within the tail. We identify regions in cis-lunar space where particles precipitate onto the lunar nightside and are carved out of the velocity distribution. This generates an extended shadow that partially shields the Moon's dayside surface from SEEs that would have otherwise mirrored near Earth and returned to the Moon, resulting in a lower electron flux on the dayside compared to the nightside. A similar process occurs in the solar wind, but the comparatively stable orientation of the magnetotail lobe field, along with the initial arrival of SEEs from down-tail, portends a more predictable cis-lunar shadow of reduced fluxes near the dayside close to the Earth-Moon line.

2. Methods

Since 2004, the Wind spacecraft (Harten & Clark, 1995) has been located $\sim 200 R_E$ upstream of Earth, providing continuous monitoring of the incoming plasma and energetic particle environment. The spacecraft's Three-Dimensional Plasma instrument (3DP; Lin et al., 1995) measures particles over a large range of energies, using an Electrostatic Analyzer (ESA) that detects electrons at energies from ~ 5 eV $\leq E \leq 30$ keV and a Solid State Telescope (SST) that observes electrons from 20 keV $\leq E \leq 1$ MeV. The two probes (P1 and P2) of the THEMIS-ARTEMIS mission (*Time History of Events and Macroscale Interactions during Substorms-Acceleration, Reconnection, Turbulence, and Electrodynamics of the Moon's Interaction with the Sun*; hereafter, ARTEMIS), which have been orbiting the Moon since 2011, have identical instrumentation including an electron ESA (5 eV $\leq E \leq 30$ keV) and SST (25 keV $\leq E \leq 1$ MeV) that share heritage with 3DP on Wind (see Angelopoulos, 2011; McFadden et al., 2008). The similarities between the instruments, the large spatial separation between the spacecraft, and the Moon's (and ARTEMIS probes') monthly transit through the magnetotail provide a unique opportunity to constrain how Earth's magnetosphere shapes the properties of incident electrons during SEE events and investigate the degree to which they are prevented from reaching the lunar surface.

To account for slight differences between the instrument calibrations and responses, we first investigate an SEE event that was observed by the three spacecraft when located within the solar wind. On 15 December 2023, SEE measurements from the Wind electron ESA and SST were a factor of 3 and 2 lower, respectively, than the ARTEMIS observations (for further detail, see Figure S1 in Supporting Information S1). To ensure the measurements have a similar baseline for comparison, we multiply the Wind observations by these calibration factors, allowing for more accuracy when quantifying the role that Earth's tail has on these electrons.

3. Results

3.1. SEE Observations Within the Tail

At 03:26 UTC on 01 September 2023, an M1.2 solar flare erupted from active region AR13413, generating a burst of SEEs. Figure 1 displays observations from Wind and ARTEMIS P2 during this event, with electron PADs included at select energies. The P2 ESA PAD (14 keV) has been sampled to a 30 s resolution to match the SST sampling rate more closely and improve signal-to-noise. To facilitate comparison, the PADs are normalized by the maximum detected flux at each time. Panel 1e provides the magnetic field in Geocentric Solar Ecliptic (GSE) coordinates, where x points from Earth toward the Sun, y lies within the ecliptic plane (opposite Earth's orbital motion), and z is normal to the ecliptic. P1 had a low sampling resolution during this time, so its observations are not included.

Figure 1 illustrates that electrons from the 01 September 2023 SEE event first arrived to Wind and P2 approximately 20 min after the flare, with a clear dispersive signature in the differential flux. The similarity between the spectra observed by the spacecraft (panel 1f) provides confidence that these electrons originated from the same source, but the omnidirectional fluxes observed by ARTEMIS are up to a factor of 1.5 higher than those observed by Wind, with the largest differences occurring for energies $E \lesssim 30$ keV. Despite the similarities between the 2-hr-averaged spectra, panels 1c and 1d highlight differences between the electron PADs. The distribution of the SEEs observed by Wind were nearly field-aligned: the pitch angles of 310 keV electrons were maximized near pitch angles of $\alpha \lesssim 45°$ while 13 keV electrons remained below $\alpha \lesssim 10°$. The field-aligned nature of these electrons for nearly 8 hr after their initial onset indicates their continual streaming outward from the Sun past the Wind spacecraft. As in panel 1a, the dispersive signature of these SEEs is visible in the electron PADs. However, the

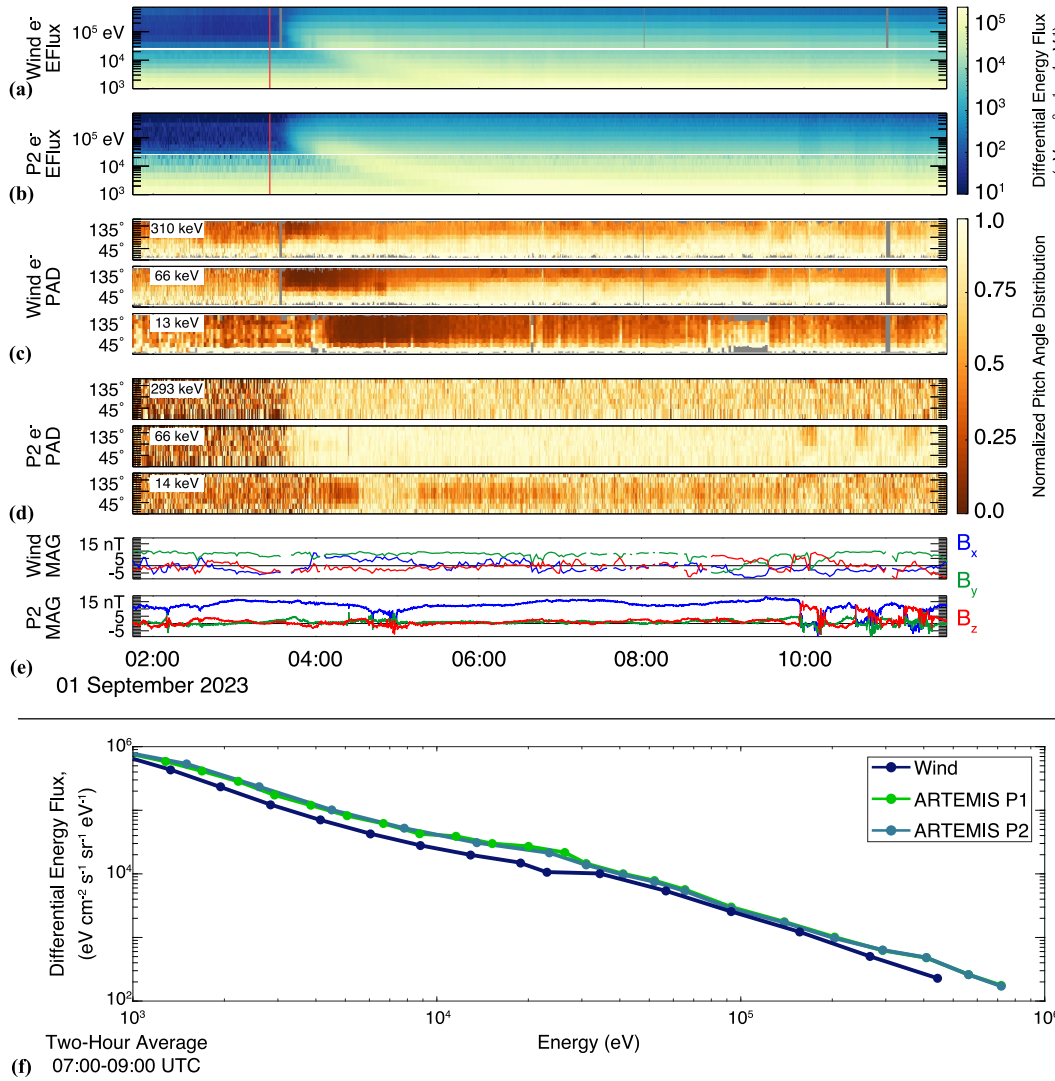

Figure 1. Solar energetic electron observations on 1 September 2023. Panels (a) and (b) display Wind and P2 differential energy fluxes, (c) and (d) show the pitch angle distributions (PADs) normalized to the maximum value at each point in time, and (e) displays the magnetic field in Geocentric Solar Ecliptic. Gray shading in (a) and (c) denotes periods without Wind data. Panel (f) shows a 2-hr average (from 07:00–09:00 UTC) of the differential energy fluxes. The vertical red lines in (a)–(b) denote the time of the M1.2 flare.

electron PADs observed by ARTEMIS were not field aligned: panel 1d instead illustrates that they were isotropic across multiple energies. The magnetic field within the tail was mainly pointed toward Earth ($B_x > 0$), so electrons originating from down-tail with pitch angles $0° \leq \alpha < 90°$ traveled Earthward as they passed the ARTEMIS probes. On the other hand, electrons with pitch angles of $90° < \alpha \leq 180°$ must have traveled *tailward* as they passed the probes. These distributions suggest that SEEs with anti-field-aligned pitch angles initially passed the Moon from down-tail and mirrored in the enhanced near-Earth field before returning to the lunar environment and being detected a second time. This is consistent with the fluxes observed by ARTEMIS being enhanced by ∼1.5 times compared to Wind. This factor being slightly less than two suggests that some of the initially Earthward-traveling electrons were scattered or lost before returning to the Moon.

Such a mechanism is further supported by the observations near 10:00 UTC. Here, P2 was located between the Earth and Moon approximately $10R_L$ above the surface and observed three brief reductions in the differential energy flux, each lasting ∼20 min (see Figures 1b and 1d). During these observations, the magnetic field rotated to be nearly aligned with the +z-direction (panel 1e), indicating that P2 was connected to a magnetosheath field line; inspection of the ESA ion fluxes during this time (not shown) also confirms the presence of magnetosheath

plasma. Since the probe was no longer on a field line connected to Earth, the mirrored component of the electron flux disappeared resulting in a drop-out of electrons at pitch angles $\alpha \geq 90°$ (panel 1d).

To further investigate this effect, Figure 2 shows electron energy fluxes (2a and 2b), PADs (2c and 2d), and magnetic field (2e) detected by ARTEMIS during a separate SEE event on 31 July 2023 (generated by an M4.1 flare and a CME that occurred 3 days earlier). Observations from Wind during this time are not included, but similar to the 01 September 2023 event, the SEEs were highly field-aligned far upstream of Earth. Even while deep within the magnetotail, the probes detected enhanced SEE fluxes as shown in Figure 2. Note that the PADs in panels 2c and 2d are not normalized, and that the 1–10 keV PADs (detected by the ESAs) have been sampled to match the temporal resolutions of the SSTs (~30 s).

As with the September event (see Figure 1), the electron PADs detected by ARTEMIS during this July event were mainly isotropic across a wide range of energies from 1 keV $\leq E \leq$ 300 keV (see panels 2c and 2d). However, both probes passed through regions where the electron fluxes dropped, with distinct bite-outs in the observed PADs. Near closest approach, P1 detected one such feature (magenta horizontal bar in Figure 2), where the electron fluxes were reduced in ESA energy channels by a factor of ~2. Since the attenuators on the ARTEMIS SSTs were activated near closest approach, there are no useable SST measurements from P1 after 18:10 UTC (gray regions in panel 2c). However, the PAD measured by ESA indicates that electrons near 18:30 UTC were initially field-aligned (i.e., depletions at pitch angles $90° < \alpha \leq 180°$ were detected), before transitioning to reductions at all pitch angles near 18:45 UTC, followed by a population of anti-field-aligned electrons at 19:20 UTC and 19:30 UTC.

Similarly, P2 detected seven such depletions in the electron fluxes (magenta bars in Figure 2). As seen in panel 2d, these flux depletions were associated with variable dropouts in the PADs, at times occurring across all pitch angles while at others occurring only for field-aligned ($0° \leq \alpha < 90°$) electrons. For example, near 15:10 UTC, the 1–10 keV electron distribution measured by the ESA on P2 was first reduced at pitch angles $0° \leq \alpha < 90°$, before displaying a full reduction across all pitch angles after 15:30 UTC. Five minutes later, the flux of only field-aligned electrons was again reduced until approximately 16:00 UTC. Similar features (but less extended in time) were detected in the pitch angles of higher-energy electrons as well. These features were not magnetospheric in origin, as the P1 electron PAD during this time was isotropic and featureless.

To determine whether each probe was connected to the Moon, we calculate the "impact parameter" (Van Allen & Ness, 1969): we project a line parallel to the observed magnetic field vector toward the lunar surface at each point. If this line intersects the surface, this parameter is $\leq 1R_L$ and the probe was connected to a field line that threaded the lunar disk. The times when this occurred are indicated by black horizontal bars in panel 2e. This approximation cannot account for changes in the magnetic field that occur *between* the probe and the Moon (e.g., crustal anomalies), but is estimated to be accurate to within 2° (~$0.07R_L$ for each $2R_L$ in altitude; see Van Allen, 1970; Van Allen & Ness, 1969). The shadows in the SEE flux across multiple pitch angles and energies closely coincide with times when the probes were magnetically connected to the lunar surface, showing a correlation between the probes' magnetic connection and the reduced SEE fluxes. This is especially visible for P1 which was only disconnected from the surface near 19:30 UTC, coinciding with a brief region where the 1–10 keV PAD showed no clear depletion, although there are larger deviations for P2 which are discussed below.

To further investigate the relationship between magnetic connectedness and the observed SEE shadows, Figure 2f displays a simplified schematic of the lunar environment in the GSE x-y plane, along with the ARTEMIS probes' trajectories, during the 31 July 2023 SEE event. The magnetospheric field was predominantly pointing down-tail (see panel 2e) and the perpendicular bulk plasma velocity was ~20 km/s, with components along the $-y$ and $-z$ axes; that is, the magnetotail was convecting southward and along the Moon's orbital direction (see Figure S2 in Supporting Information S1).

Assuming the SEEs during the 31 July 2023 event entered Earth's magnetotail from far downstream, electrons approaching the Moon from down-tail and located within the region defined by $\sqrt{y^2 + z^2} \leq R_L$ would impact the nightside lunar surface (gray half-circle in Figure 2f). An Earthward-traveling electron located just outside of this cylinder near the dusk terminator (with pitch angle $\alpha = 180°$) would just pass the lunar surface without impacting (green arrow labeled "Final Earthward SEE" in panel 2f). Ignoring pitch angle scattering, this electron would mirror near the Earth and travel back toward the Moon with a pitch angle of $\alpha = 0°$ (green "Final reflected SEE"). In the finite time required for the electron to travel the ~$120R_E$ round-trip, the magnetic field line along which the

10.1029/2024GL110228

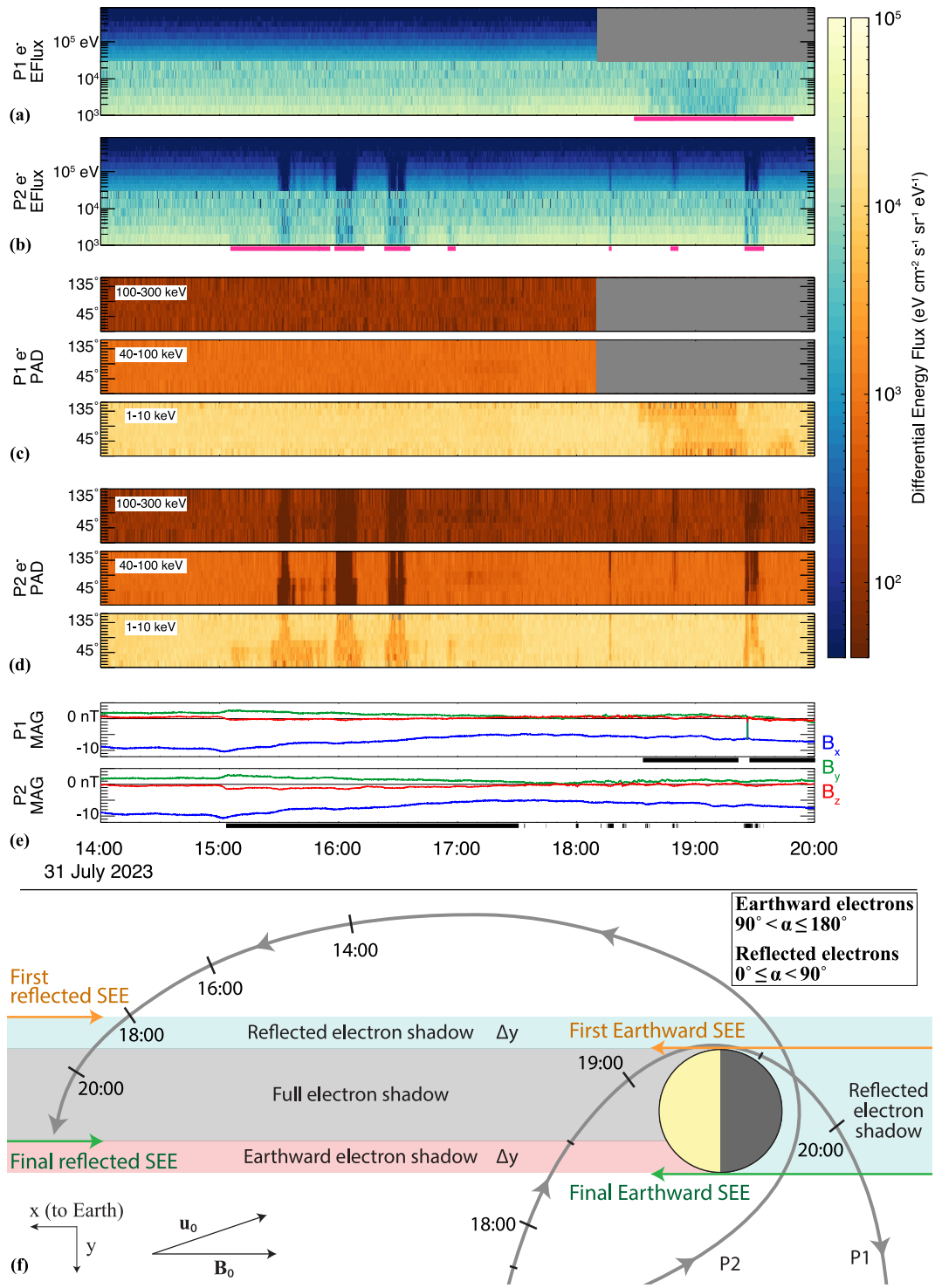

Figure 2. ARTEMIS solar energetic electron (SEE) observations on 31 July 2023 within Earth's southern magnetotail lobe. Black bars along the bottom of (e) show times where the probes were magnetically connected to the lunar surface, while magenta bars in (a) and (b) indicate regions depleted of SEEs. The P1 data gap at high energies corresponds to closest approach, where the Solid State Telescope attenuator was activated. Panel (f) displays a schematic explaining the SEE drop-outs, projected onto the Geocentric Solar Ecliptic *x*-*y* plane and viewed from above the Moon's North pole. Colored regions correspond to SEE shadows, for (blue) reflected electrons, (red) Earthward electrons, and (gray) all electrons, and Δy indicates the electron's displacement in the $-y$-direction caused by magnetotail convection.

electron is bouncing has convected a distance Δy along the $-y$ axis, and this electron would impact the dayside lunar surface. The width Δy of this region is energy-dependent, ranging from $0.35R_L$ to $0.03R_L$ for electrons with initially aligned pitch angles that mirror at Earth with energies between 1 keV $\leq E \leq$ 300 keV. In cis-lunar space, this process therefore generates a void in the distribution of *Earthward*-traveling electrons (red shading in panel 2f; see also Van Allen, 1970).

Similarly, we can consider an Earthward-traveling electron initially down-tail of the Moon and near the dawn terminator that lies just outside the region defined by $\sqrt{y^2 + z^2} \leq R_L$. This electron would travel past the Moon without impacting the lunar surface (labeled "First Earthward SEE" in orange), reflect near Earth, and return to the Moon. Again, the convection of the magnetotail causes a displacement of Δy for this electron along the Moon's orbital direction, generating a shadow of *reflected* electrons (blue shading in panel 2f). Between these two regions, *no* SEEs are present in cis-lunar space: Earthward-traveling electrons would have impacted the lunar nightside surface, so a drop-out in electrons forms at all pitch angles.

Panel 2f shows that for this simplified scenario, P1 would first encounter a shadow of Earthward-traveling ($90° < \alpha \leq 180°$) electrons near 18:00 UTC, followed by a drop-out at all pitch angles, and finally a shadow in reflected SEEs ($0° \leq \alpha < 90°$) after passing into the nightside. For P2, Figure 2f suggests the reverse order since its orbit direction is counter-clockwise compared to the clockwise orbit of P1: first, P2 would detect a shadow of reflected electrons, then across all pitch angles, followed by a drop-out for the Earthward-traveling electrons.

Figures 2a–2d show that the ARTEMIS observations of electron shadows are consistent with this behavior. P1 was connected to the lunar surface for approximately 1.5 hr beginning near 18:30 UTC, where ESA observed a reduction in the differential electron flux (the SST attenuator was engaged so higher-energy electrons were not measured). The PAD of these electrons is consistent with the shadow behavior illustrated in Figure 2f: an initial drop-out in the Earthward-traveling electrons ($90° < \alpha \leq 180°$) was observed, followed by a reduced flux at all pitch angles from 18:42 UTC through 19:20 UTC, when the probe crossed into the lunar nightside. After this point, the probe encountered a reflected electron shadow, characterized by reduced fluxes of $0° \leq \alpha < 90°$ electrons until approximately 19:50 UTC. The electron flux was briefly filled in near 19:30 UTC, coinciding with the time that P1's magnetic connection to the surface was temporarily disrupted as the probe crossed the lunar terminator.

Using the observed shadows, we can estimate the convection velocity of the tail. The shadow of Earthward-traveling, 1–10 keV electrons initially detected by P1 between 18:30 UTC and 18:42 UTC had a width of $\Delta y = 0.39R_L$ along P1's orbit. The time for a field-aligned, 1 keV electron to travel from the Moon to its mirror point at Earth ($60R_E$ away) and back is 41 s, while a 10 keV electron completes this round-trip in 13 s. These values, along with the observed width of the shadow, suggest that the tail convection velocity was between 16 km/s and 50 km/s along the y-direction, which is consistent with the ARTEMIS observations of the cold, $\mathbf{E} \times \mathbf{B}$ drifting ion population at this time (see Figure S2 in Supporting Information S1).

For P2, the probe was estimated to be magnetically connected to the lunar surface beginning near 15:10 UTC, where it detected a shadow in the reflected electron population (pitch angles $0° \leq \alpha < 90°$) that was sustained for ∼30 min. This drop-out was initially detected in the ESA for 1–10 keV electrons, before extending to the SST instrument at energies 40–100 keV. Near 15:30 UTC, a drop-out at all pitch angles was observed for ∼5 min at energies 1 keV $\leq E \leq$ 300 keV, after which the probe again passed through a reflected electron shadow. Similar features, alternating between reflected and full electron shadows, were observed by P2 until approximately 17:00 UTC. Finally, near 19:30 UTC, P2 again detected a drop-out across all electron pitch angles, followed by a brief detection of a reflected electron shadow.

Despite the promising agreement between the schematic in Figure 2f and the electron PADs observed by P1, there are deviations from this simplified picture for P2. Although the impact parameter calculation suggests that P2 was connected to the surface continuously from 15:00–17:30 UTC, the probe did not detect a single shadow during this time. Instead, P2 measured distinct intervals of shadowing that were separated by up to 30 min. In addition, the first observed shadow was seen approximately 2.5 hr earlier than Figure 2f suggests. These discrepancies are likely caused by changes in the magnetic field vector between the spacecraft and surface and non-uniform magnetotail convection patterns during this time (including convection out of the plane displayed in Figure 2f), which caused this magnetic connection to be severed. Besides, since P2 was located ∼$10R_L$ from the

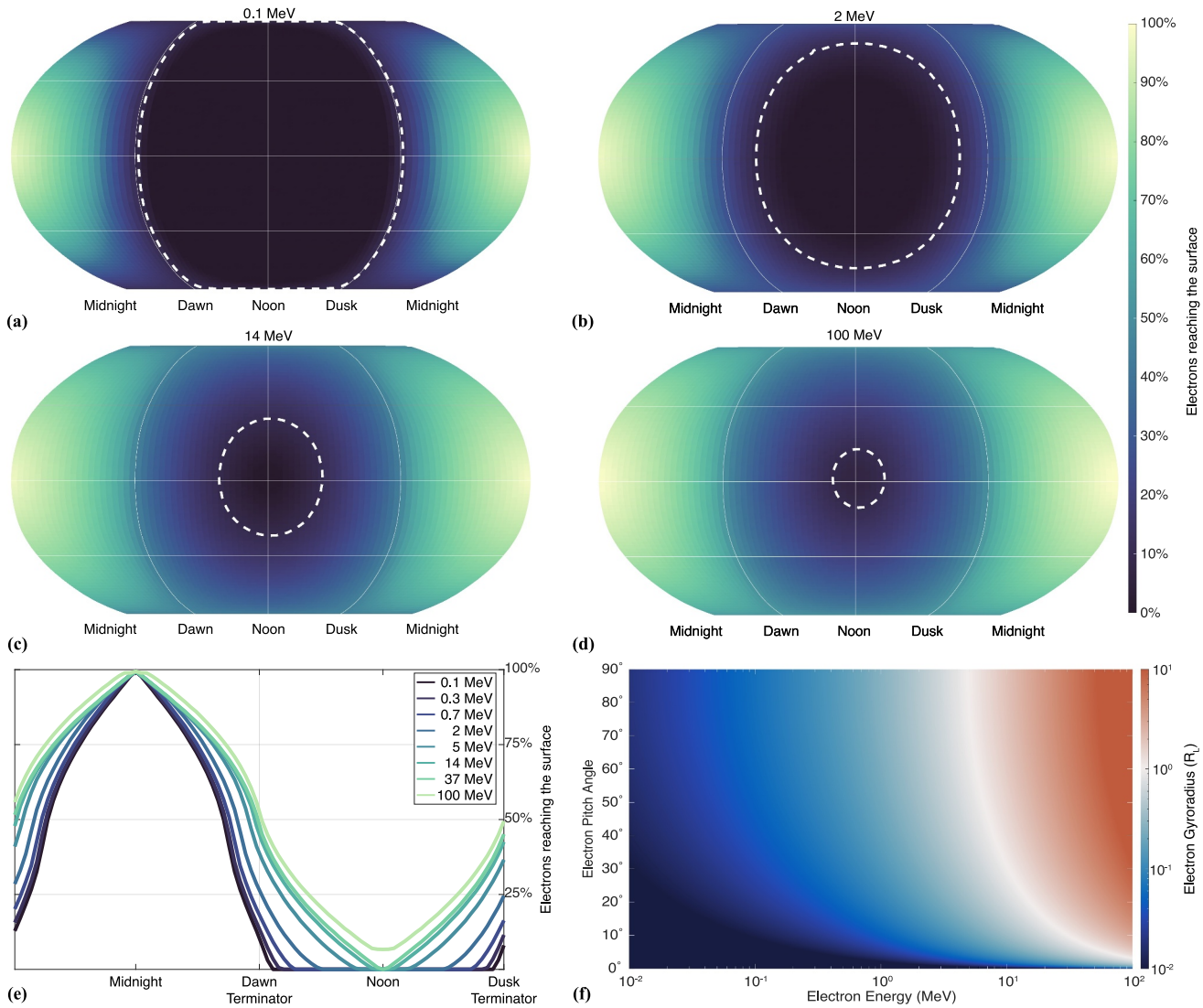

Figure 3. Relativistic electron (a–d) precipitation maps with the 10% contour given by the dashed-white line, (e) equatorial access at select energies, and (f) pitch angle and gyroradii.

Moon, there are large uncertainties (up to $0.35R_L$) in the impact parameter calculation. Regardless, Figure 2 shows evidence for SEE shadowing by the lunar surface that are sustained through extended regions of the magnetotail.

3.2. Modeling SEE Access to the Lunar Surface

To determine locations across the lunar surface that are accessible to initially Earthward-traveling SEEs, we modeled the precipitation patterns of these electrons using the relativistic GENTOo model (Liuzzo et al., 2019a), which has been applied for studies of multiple moons throughout the solar system (e.g., Addison et al., 2021, 2022; Breer et al., 2019; Liuzzo et al., 2019b, 2020; Liuzzo, Nénon, et al., 2024; Liuzzo, Poppe, Addison, et al., 2022; Liuzzo, Poppe, et al., 2024). For select energies, electrons were initialized at a given a velocity (determined by the particle's energy), pitch angle (with a resolution of 2°), and gyrophase (with a 4° resolution), and their dynamics are modeled while they remain within a distance of $\sim 10R_L$ from the lunar surface; that is, we do not consider electrons that are mirrored near Earth. We aligned the magnetic field with the GSE $-x$ axis with a magnitude of $|\mathbf{B}| = 10$ nT and assumed no perpendicular convection, consistent with typical magnetotail lobe conditions (see Liuzzo, Poppe, & Halekas, 2022; Runov et al., 2023).

Figures 3a–3d display the percentages of Earthward-traveling SEEs that precipitate onto a given location on the lunar surface for select energies ranging from 100 keV $\leq E \leq$ 100 MeV. Although this upper limit extends beyond the energy range detectable by ARTEMIS and Wind, it allows us to investigate precipitation patterns for electrons whose gyroradii exceed the size of the Moon. Figure 3e shows this percentage along the equator for various electron energies, while Figure 3f illustrates the relativistic electron gyroradii as a function of pitch angle. As visible in panel 3a, nearly all the 0.1 MeV electrons (gyroradii $r_g \leq 0.06R_L$) precipitate onto the nightside (trans-lunar) surface. To illustrate this further, the white dashed line in panel 3a denotes the contour where only 10% of electrons reach the surface. Since their gyroradii are small compared to the size of the Moon, only few 0.1 MeV electrons that originate from down-tail precipitate onto the dayside and this contour is nearly co-located with the terminators (marked "dusk" and "dawn"). This nightside precipitation forms the electron shadows in cis-lunar space, as detected by ARTEMIS when magnetically connected to the Moon (see Figure 2).

The precipitation patterns are qualitatively similar across multiple energies (see panels 3b–3d), with access of Earthward-traveling SEEs gradually expanding into the cis-lunar hemisphere with increasing energy. The growing gyroradii allows an increasing fraction of electrons near perpendicular pitch angles to reach beyond the terminator and the 10% accessibility contours approach the subsolar point. However, even with gyroradii that eventually exceed the radius of the Moon by an order of magnitude for the highest energy studied here, Earthward-traveling SEEs still do not uniformly irradiate the surface, with only ∼10% of 100 MeV electrons reaching the subsolar point (which here coincides with the region where the magnetic field vector is normal to the Moon's surface). Indeed, the access of SEEs to the equatorial lunar dayside drops precipitously when crossing the terminators, regardless of particle energy (panel 3e).

There are several caveats associated with interpretation of Figure 3. For example, we assume the ambient magnetic field is uniform and oriented in the $-x$-direction (anti-Sunward), which is representative of the local magnetospheric field within the magnetotail lobes (Liuzzo, Poppe, & Halekas, 2022; Liuzzo et al., 2021) but does not hold true over scales of multiple R_E, and we have ignored perpendicular drifts over similar length scales. Changes to the electrons' trajectories associated with these effects are not represented in this approach, and we caution that these results should *not* be interpreted as a complete lack of electron precipitation across the dayside surface. However, these results are consistent with observations of electron shadows in cis-lunar space that reduce precipitation of SEEs onto the dayside when the Moon is in the tail as shown in Figures 1 and 2.

4. Discussion and Conclusions

We have focused on two case-studies to show that SEEs access the lunar environment even when embedded within the terrestrial magnetotail. For two separate SEE events, we find that the tail is open to these particles with fluxes that were nearly unaltered compared to their distribution upstream and show that they have direct access to the lunar nightside surface. Finally, we have identified electron shadows that extend through cis-lunar space, where structured and sustained drop-outs in the flux of Earthward-traveling and (reflected) tailward-traveling SEEs span multiple orders of magnitude in energy. Importantly, while our findings suggest that the lunar dayside surface flux is relatively reduced compared to the flux onto the nightside during SEE events, these results indicate that high-energy electrons during solar particle events have direct access to the lunar orbit within the magnetotail. A detailed comparison between the temporal dispersion in the SEE arrival times at Wind and ARTEMIS across a range of energies would allow for a greater understanding of where these electrons gain access to the magnetotail, but this is not possible for these events due to the instruments' sample rates.

Multiple identifications of these electron shadows by ARTEMIS indicate they are common features during SEE events; a table and additional observations are provided in Supporting Information S1. Electron shadows were also seen by Explorer 35, with Lin (1968) and Van Allen and Ness (1969) suggesting that they preferentially occur in cis-lunar space within a few radii of the Moon's surface when in the magnetotail. However, we have shown that shadows in Earthward-traveling electrons extend far from the surface and are clearly identifiable in particle data taken at least ∼$10R_L$ from the Moon. In addition, we have illustrated that Earthward-traveling SEEs can pass the Moon, be reflected in the enhanced field near Earth, and precipitate onto the lunar dayside. Not only does this behavior tend to isotropize the SEE population within the magnetotail, but it generates an additional electron shadow in trans-lunar space. The reduced flux of this reflected (tailward-traveling) population suggests that the shadows must persist at distances $\gg 10R_L$ from the Moon. Hence, we propose that the only requirement for future detections of these shadows is a magnetic connection to the lunar surface during a SEE event, with some portion

of the population counter-streaming across the opposite side of the Moon. There is therefore no stipulation for isotropy (or lack thereof) of the incident electron population to generate these shadows in the particle distribution (cf. Anderson & Lin, 1969; Van Allen, 1970). These results are important for the fundamental scientific understanding of SEEs and their access to the lunar surface. In addition, our findings have important implications in the context of exploration of the near-lunar environment by the upcoming crewed Artemis and Lunar Gateway missions.

Data Availability Statement

THEMIS-ARTEMIS data are available at sprg.ssl.berkeley.edu/data/themis and Wind data can be accessed at sprg.ssl.berkeley.edu/data/wind. Analysis software for ARTEMIS is available through the Space Physics Environment Data Analysis Software (Angelopoulos et al., 2019) and analysis software for Wind can be found at Wilson (2021).

Acknowledgments
The authors are supported by NASA Lunar Data Analysis Program Grant 80NSSC23K1338. L.L. thanks L.B. Wilson III for insight into Wind 3DP. The authors acknowledge NASA contract NAS5-02099 for the use of ARTEMIS data, and specifically, J.P. McFadden for use of ESA data and K.-H. Glassmeier, U. Auster, and W. Baumjohann for the use of FGM data provided under the lead of the Technical University of Braunschweig with financial support through the German Ministry for Economy and Technology and the German Center for Aviation and Space, Contract 50-OC-0302.

References

Addison, P., Liuzzo, L., Arnold, H., & Simon, S. (2021). Influence of Europa's time-varying electromagnetic environment on magnetospheric ion precipitation and surface weathering. *Journal of Geophysical Research: Space Physics*, *126*(5), 1–42. https://doi.org/10.1029/2020JA029087

Addison, P., Liuzzo, L., & Simon, S. (2022). Effect of the magnetospheric plasma interaction and solar illumination on ion sputtering of Europa's surface ice. *Journal of Geophysical Research: Space Physics*, *127*(2), 1–39. https://doi.org/10.1029/2021JA030136

Anderson, K. A., & Lin, R. P. (1969). Observation of interplanetary field lines in the magnetotail. *Journal of Geophysical Research*, *74*(16), 3953–3968. https://doi.org/10.1029/JA074i016p03953

Angelopoulos, V. (2011). The ARTEMIS Mission. *Space Science Reviews*, *165*(1–4), 3–25. https://doi.org/10.1007/s11214-010-9687-2

Angelopoulos, V., Cruce, P., Drozdov, A., Grimes, E. W., Hatzigeorgiu, N., King, D. A., et al. (2019). The Space Physics Environment Data Analysis System (SPEDAS). *Space Science*, *215*(1), 9. The Author(s). https://doi.org/10.1007/s11214-018-0576-4

Breer, B. R., Liuzzo, L., Arnold, H., Andersson, P. N., & Simon, S. (2019). Energetic ion dynamics in the perturbed electromagnetic fields near Europa. *Journal of Geophysical Research: Space Physics*, *124*(9), 7592–7613. https://doi.org/10.1029/2019JA027147

Harten, R., & Clark, K. (1995). The design features of the GGS wind and polar spacecraft. *Space Science Reviews*, *71*(1–4), 23–40. https://doi.org/10.1007/BF00751324

Jordan, A. P., Wilson, J. K., & Spence, H. E. (2023). Energetic charged particle dose rates in water ice on the Moon. *Icarus*, *395*, 115477. https://doi.org/10.1016/j.icarus.2023.115477

Lin, R. P. (1968). Observations of lunar shadowing of energetic particles. *Journal of Geophysical Research*, *73*(9), 3066–3071. https://doi.org/10.1029/JA073i009p03066

Lin, R. P., Anderson, K. A., Ashford, S., Carlson, C., Curtis, D., Ergun, R., et al. (1995). A three-dimensional plasma and energetic particle investigation for the Wind spacecraft. *Space Science Reviews*, *71*(1–4), 125–153. https://doi.org/10.1007/BF00751328

Liuzzo, L., Nénon, Q., Poppe, A. R., Stahl, A., Simon, S., & Fatemi, S. (2024). On the formation of trapped electron radiation belts at Ganymede. *Geophysical Research Letters*, *51*(10), e2024GL109058. https://doi.org/10.1029/2024GL109058

Liuzzo, L., Poppe, A. R., Addison, P., Simon, S., Nénon, Q., & Paranicas, C. (2022). Energetic magnetospheric particle fluxes onto Callisto's atmosphere. *Journal of Geophysical Research: Space Physics*, *127*(11), 1–30. https://doi.org/10.1029/2022JA030915

Liuzzo, L., Poppe, A. R., & Halekas, J. S. (2022). A statistical study of the Moon's magnetotail plasma environment. *Journal of Geophysical Research: Space Physics*, *127*(4), 1–23. https://doi.org/10.1029/2022JA030260

Liuzzo, L., Poppe, A. R., Halekas, J. S., Simon, S., & Cao, X. (2021). Investigating the Moon's interaction with the terrestrial magnetotail lobe plasma. *Geophysical Research Letters*, *48*(9), 1–11. https://doi.org/10.1029/2021GL093566

Liuzzo, L., Poppe, A. R., Lee, C. O., Xu, S., & Angelopoulos, V. (2023). Unrestricted solar energetic particle access to the moon while within the terrestrial magnetotail. *Geophysical Research Letters*, *50*(12), 1–9. https://doi.org/10.1029/2023GL103990

Liuzzo, L., Poppe, A. R., Nénon, Q., Simon, S., & Addison, P. (2024). Constraining the influence of Callisto's perturbed electromagnetic environment on energetic particle observations. *Journal of Geophysical Research: Space Physics*, *129*(2), e2023JA032189. https://doi.org/10.1029/2023JA032189

Liuzzo, L., Poppe, A. R., Paranicas, C., Nénon, Q., Fatemi, S., & Simon, S. (2020). Variability in the energetic electron bombardment of Ganymede. *Journal of Geophysical Research: Space Physics*, *125*(9), 1–35. https://doi.org/10.1029/2020JA028347

Liuzzo, L., Simon, S., & Regoli, L. (2019a). Energetic electron dynamics near Callisto. *Planetary and Space Science*, *179*(August), 104726. https://doi.org/10.1016/j.pss.2019.104726

Liuzzo, L., Simon, S., & Regoli, L. (2019b). Energetic ion dynamics near Callisto. *Planetary and Space Science*, *166*, 23–53. https://doi.org/10.1016/j.pss.2018.07.014

McFadden, J. P., Carlson, C. W., Larson, D., Ludlam, M., Abiad, R., Elliott, B., et al. (2008). The THEMIS ESA plasma instrument and in-flight calibration. *Space Science Reviews*, *141*(1–4), 277–302. https://doi.org/10.1007/s11214-008-9440-2

Runov, A., Angelopoulos, V., Khurana, K., Liu, J., Balikhin, M., & Artemyev, A. V. (2023). Properties of quiet magnetotail plasma sheet at lunar distances. *Journal of Geophysical Research: Space Physics*, *128*(11), e2023JA031908. https://doi.org/10.1029/2023JA031908

Terada, K., Yokota, S., Saito, Y., Kitamura, N., Asamura, K., & Nishino, M. N. (2017). Biogenic oxygen from Earth transported to the Moon by a wind of magnetospheric ions. *Nature Astronomy*, *1*(2), 0026. https://doi.org/10.1038/s41550-016-0026

Van Allen, J. A. (1970). Energetic particle phenomena in the Earth's magnetospheric tail. In B. M. McCormac (Ed.), *Particles and fields in the magnetosphere* (Vol. 17, pp. 111–121). Springer Netherlands. https://doi.org/10.1007/978-94-010-3284-1

Van Allen, J. A., & Ness, N. F. (1969). Particle shadowing by the Moon. *Journal of Geophysical Research*, *74*(1), 71–93. https://doi.org/10.1029/JA074i001p00071

Wilson, L. B. (2021). lynnbwilsoniii/wind_3dp_pros: Space plasma missions IDL software library [Software]. *Zenodo*. https://doi.org/10.5281/zenodo.4451330